9.13   Solar radiation budget derived by integrating ground-based and satellite observations with a Monte Carlo radiation model

Dohyeong Kim[1], V. Ramanathan[1], Atsumu Ohmura[2], and Ellsworth G. Dutton[3]

Center for Clouds, Chemistry and Climate (C[4]), Scripps Institution of Oceanography, La Jolla CA. 92093[1],
Geographisches Institut, ETH, Zurich, Switzerland[2],
NOAA/Climate Monitoring and Diagnostics Laboratory, Boulder, Colorado[3]

1. INTRODUCTION

A number of studies [e.g., *Stanhill and Cohen*, 2001; *Liepert*, 2002; *Ramanathan et al.*, 2005] also show a significant reduction in solar radiation at the surface during the past 50 years. The reduction in the surface solar radiation profoundly influences evaporation, surface temperature, and the hydrological cycle [e.g., *Ramanathan et al.*, 2001; *Roderick and Farquhar*, 2002; *Ohmura and Wild*, 2002]. Most studies explain that the sunlight reduction results from an increase in optical depth due to aerosol loading (anthropogenic) and cloud cover frequency. Numerous studies [e.g., *Rotstayn and Lohmann*, 2002] have also pointed out that anthropogenic aerosols can play a role in the "drying" of the planet by heating the atmosphere. Aerosols can reduce global average precipitation by reducing the solar radiation reaching the surface. Moreover, the presence of clouds can significantly change the radiative impact of aerosols, especially when absorbing aerosols are located above the clouds [e.g., *Liao and Seinfeld, 1998*; *Haywood and Ramaswamy*, 1998; *Myhre et al.*, 2003]. Therefore, it appears that understanding the role of aerosol/cloud in solar radiation is a key to understanding the observed changes in solar radiation.

In spite of efforts to estimate the role of aerosol/clouds in global solar radiation, there is a large discrepancy in model results since there are many inherent assumptions involved in simulating the aerosol/cloud effect on climate. The uncertainties come mainly from assumptions concerning the physical and chemical properties of aerosols as well as aerosol-cloud interactions. Reduction of these uncertainties in global studies requires an integrated approach using multiple data sources, e.g., ground-based, satellite, and model retrieved data [e.g., *Boucher and Tanre*, 2000; *Chou et al.*, 2002; *Christopher and Zhang*, 2002; *Yu et al.*, 2004].

Our main objectives are to accurately simulate the measured solar radiation at both the surface and the top of the atmosphere (TOA), and to quantify the role of aerosol/cloud in the global solar radiation field. For this purpose, we use the Monte Carlo Aerosol-Cloud-Radiation (MACR) model developed by the Center for Clouds, Chemistry and Climate (C[4]) at the University of California San Diego [*Podgorny et al.*, 2000; *Podgorny and Ramanathan*, 2001; *Vogelmann et al.*, 2001; *Chung et al.*, 2005). For aerosol parameters (aerosol optical depth, single scattering albedo, and asymmetry factor), the quality assured level 2.0 data from the AERONET was used [e.g., *Dubovik et al.*, 2000; *Holben et al.*, 2001; *Dubovik et al.*, 2002]. The Multi-angle Imaging SpectroRadiometer (MISR) global AODs [*Diner et al.*, 1998; *Kahn et al.*, 2001] are assimilated with AERONET for global distribution of AODs. The International Satellite Cloud Climatology Project (ISCCP)-D1 3-hour cloud data [*Rossow and Schiffer*, 1999] are used for cloudy sky flux calculation.

2. DATA

For the MACR model validation, both daily and monthly mean values at a given validation site were used. However, climatological monthly mean values on a spatial T42 grid (approximately 2.8° by 2.8°) were used for the estimation of global solar radiation budget.

2.1 Model input data

The AERONET is a worldwide network of ground-based, automated sun photometers deployed by the NASA Goddard Space Flight Center since 1993 [*Holben et al.*, 1998; *Holben et al.*, 2001]. The AERONET provides data on spectral aerosol properties and precipitable water. AERONET measurement uncertainties are well understood [e.g., *Dubovik et al.*, 2000], and the data are widely used as a standard for satellite aerosol retrieval validation. Thus, the aerosol parameters and uncertainties are suitable for model validation. The quality assured level 2 data product for aerosol optical depth (AOD), single scattering albedo (SSA) and asymmetry factor was used. The wavelength dependence of the parameters is used to incorporate the parameters with broadband wavelength ranges in the model.

MISR on the NASA Terra platform has been producing AOD measurements globally since February 2000. MISR can retrieve aerosol properties over a variety of terrain, including highly reflective surfaces like deserts, since the blend of directional and spectral data allow aerosol retrieval algorithms to be used that do not depend on explicit radiometric surface properties [*Martonchik et al.*, 2004].

The ISCCP within the World Climate Research Programme (WCRP) has been collecting infrared and visible radiances obtained from imaging radiometers carried on the international constellation of weather satellites since July 1983 [*Rossow and Schiffer*, 1999]. The 15 cloud types in the ISCCP dataset are classified into 4 cloud types: low, middle, high, and

deep convective clouds.

For model validation, the diurnal averaged dataset of cloud parameters was made from the 3 hour ISCCP D1 dataset at every grid point (2.5° by 2.5°) from 2000 to 2001. After diurnal averaging, the grid values were interpolated from BSRN station values by weighting the distance from the surrounding grid points. For global solar radiation budget, the ISCCP D2 was used, which is the monthly mean of the ISCCP D1 dataset.

2.2 Validation data

The Baseline Surface Radiation Network (BSRN) operation started in 1992 to provide validation data for satellite observations and estimated radiation code, and to monitor long-term changes in surface irradiation. At present, there are 35 BSRN stations in operation.

For the purpose of more reasonable model validation, stations measuring both global and diffuse fluxes were used to apply the clear sky detection algorithm. Stations were selected which measured all the BSRN data, i.e., AERONET measurements for AOD, SSA, asymmetry factor, water vapor from radiosonde, total ozone amounts from TOMS, and cloud parameters from ISCCP D1.. These strict criteria significantly reduced the number of stations. The selected stations (Barrow [71.3°N, 156.6°W], Bermuda [32.3°N, 64.8°W], Billings [36.6°N, 97.51°W], Bondville [40.1°N, 88.4°W], Nauru Island [0.5°S, 166.9°E], and Solar Village [24.9°N, 46.4°E]) are given in Figure 1.

The Clouds and the Earth's Radiant Energy System (CERES) data was used for the validation of model calculations at the TOA. The ERBE-like CERES ES-9 product, which used the algorithm for the Earth Radiation Budget Experiment (ERBE), was adopted.

3. RADIATIVE TRANSFER MODEL

For the validation study, the model inputs are based on daily mean values at each station. Model inputs were confined by measurements obtained at a given station, but some were interpolated from surrounding grids if the data were not available at a given station. For the global radiation budget calculation, the model was deployed on the T42 grid (approximately 2.8º by 2.8º resolution) and run using monthly mean basis inputs.

3.1 Description of model

The model used in this study is the Monte-Carlo Aerosol Cloud Radiation (MACR) model [*Satheesh et al.,* 1999; *Ramanathan et al.,* 2001]. Recently the MACR model has been updated in order to enable it to produce global predictions using observational input data, such as aerosol optical parameters, total ozone amount, precipitable water, surface albedo, and cloud parameters. In addition, the model accounts for the surface orography, all multiple scattering and absorption by individual aerosol species, cloud droplets, air molecules, and reflections from the surface. The model uses 25 bands to cover the solar spectrum from 0.25 to 5.0 μm with 50 layers [*Vogelmann et al.,* 2001].

3.2 Atmospheric absorption

The correlated k-distributions (referred to CK) [e.g., *Lacis and Oinas,* 1991; *Fu and Liou,* 1992; *Kato et al.,* 1999] are used to incorporate gaseous absorption by water vapor, ozone, oxygen, and carbon dioxide. The CK is generated for 50 layers and 25 spectral regions based on the 2000 version of high-resolution transmission molecular absorption database (HITRAN 2000 database). The water vapor continuum absorption based on the algorithm given by *Clough et al.* [1989] is also incorporated in the CK [*Stephens and Tsay,* 1990; *Vogelmann et al.,* 1998].

For the atmospheric gases, the vertically-integrated amount of ozone from 1979 to 2000 was derived from TOMS. The Water Vapor Project (NVAP) total column water vapor datasets from 1988 to 2002, which are obtained from the NASA Langley Research Center Atmospheric Sciences Data Center, was used.

3.3 Cloud absorption/scattering

We used the measured cloud optical depth and cloud fraction from ISCCP global cloud data, which were combined into four different types, low, mid, high and convective clouds. The random/maximum cloud overlap scheme was adopted for treatment between low, mid and high clouds [*Chen et al.*, 2000]. Deep convective clouds were explicitly taken into account. Cloud SSA and asymmetry factor have been computed using Optical Properties of Aerosols and Clouds (OPAC) software [*Hess et al.,* 1998].

3.4 Surface reflection

The land surface albedo was obtained from the European Centre for Medium-Range Weather Forecasts (ECMWF) surface solar radiation reanalysis (1998–2001 mean). To account for the spectral dependence of vegetation albedo, the four narrowband spectral reflectivities were combined into two narrowband spectral reflectivities followed by the spectral pattern in *Briegleb et al.* [1986]. The ocean surface albedo, adopted the scheme given in *Briegleb et al.* [1986]. The ocean surface albedo was expressed by the cosine solar zenith angle, and yielded 2.5% of surface albedo when the sun was overhead, while more than 20% of the albedo for larger solar zenith angles, typically around 80 degrees. The albedo over sea ice surfaces was derived from visible ISCCP albedo. The broadband sea ice albedo was set to 80% of the visible ISCCP albedo.

4. MODEL VALIDATION AT BSRN STATIONS

Collocated BSRN stations with AERONET for

the period from 2000 and 2002 were chosen. The period from 2000 to 2002 was selected because the CERES TOA fluxes were available for model validation at TOA.

Figure 2 compares diurnal mean reflected solar flux at the TOA and surface global (direct plus diffuse) fluxes between observations and MACR under clear and cloudy sky conditions. At the surface MACR overestimates the clear sky global flux by 4.9 Wm^{-2} with an RMS errors of 6.8 Wm^{-2}. For the reflected solar flux at the TOA, MACR estimates are within 1 Wm^{-2}, but the RMS error is still large at 6.4 Wm^{-2}. The sensitivity test showed that the maximum uncertainty of diurnal mean flux at the surface was around 4 Wm^{-2}, and the uncertainty was increased with increase in AOD. The 10 % error of column water vapor amount and total ozone amount could cause 1-2 Wm^{-2} uncertainty of the incoming surface fluxes. The overall uncertainty of the MACR estimates at the surface due to the uncertainties of input parameters could be 5-6 Wm^{-2}. At the surface the MACR could estimate the clear sky flux within the uncertainty of instrument.

The MACR overestimates cloudy sky global flux by 7.3 Wm^{-2} with an RMS errors of 22.2 Wm^{-2}. For the reflected global flux at the TOA the MACR estimates are within 1 Wm^{-2} with decreased RMS error of 11.5 Wm^{-2}. Considering the fact that the MACR estimated the clear sky flux with much small uncertainty, the large errors under cloudy sky conditions might come mainly from the uncertainties of cloud optical depth and cloud fraction: 1) the uncertainty of cloud amounts is within 0.05, and the cloud optical depth has error range within 10% [*Rossow and Schiffer*, 1999]. At the surface the uncertainties of cloud parameters could change global flux around 6.0±1.4 Wm^{-2} (2.0±0.6%) from sensitivity test. For the reflected TOA flux, the error could be around 5.0±1.0 Wm^{-2} (5.0±1.4%). 2) The ISCCP cloud parameters were interpolated to each BSRN station from the nearest 2.5° by 2.5° grid points. 3) Daily and monthly mean cloud properties were used for the flux calculation. The temporal changes of cloud properties, however, were much faster than the time scales of day and month, and all the temporal changes were embedded in the measured fluxes. For the reflected global TOA flux the mean bias is around +5.5 Wm^{-2} with decreased RMS error of 6.7 Wm^{-2}, even though the interpolation error is still remained in the calculation.

5. GLOBAL SOLAR RADIATION BUDGET

The MACR model retrievals were compared with GEBA observations, with CERES data (2000-2002 average), and with the ERBE data (1985-1989 average) [*Harrison et al.*, 1990; *Ramanathan et al.*, 1989].

5.1 Comparison with satellite data (ERBE and CERES)

For the MACR global estimates the integrated global AOD and SSA data were used as inputs.

The MACR estimates at the TOA were compared with satellite retrievals (CERES and ERBE). The comparison of the annual/zonal mean clear sky TOA flux between MACR, CERES, and ERBE is presented in Figure 3. A large discrepancy was found in the southern extra tropics where the MACR overestimated the CERES retrieved fluxes over land by around 5 Wm^{-2}. In contrast, the MACR underestimated CERES fluxes over ocean by around 5 Wm^{-2}. The ERBE fluxes were higher than the MACR estimates throughout the whole latitudes.

The global annual mean flux difference between satellite data (ERBE minus CERES) was around +5 Wm^{-2} (+9%) under clear sky, and +4.5 Wm^{-2} (+4%) under cloudy sky. For clear sky flux these differences might partly come from the different time period between ERBE (1985-1989) and CERES (2000-2002), which could cause changes to surface albedo, especially in polar regions, or gaseous amount in the atmosphere. The large difference may also be explained by the different field of view resolution. The resolution of CERES was 20 km and that of ERBE was 40 km at nadir, such that the surface area observed by ERBE was 4 times larger than that of CERES. Therefore, CERES was observing more clear sky scenes than ERBE due to the difference in footprint size (CERES Quality Summary: http://eosweb.larc.nasa.gov/).

5.2 Aerosol and cloud radiation forcing

The global mean AOD was 0.150 and the global mean SSA was 0.95. Figure 4 presents the annual mean aerosol radiative forcing estimated by running the model with clouds. In general, the TOA forcing was negative, but areas where the surface albedo was high, such as over ice fields or desert, showed a positive or small negative forcing. The largest atmospheric and negative surface forcings were found over Eastern China India, Mexico, and equatorial Africa also had a large atmospheric heating and surface cooling. The clear sky aerosol forcing and the cloudy sky forcing have similar patterns, although the magnitude of forcing differs somewhat. In Figure 4 the subtropical ocean of East Africa has small negative or positive TOA forcing. It could be interpreted by the low SSA around 0.89 and the presence of low clouds over the region. The global mean clear sky TOA forcing was -5.0 Wm^{-2}, but the presence of clouds decreased the negative TOA forcing from -5.0 to -2.6 Wm^{-2}. Similarly, the negative surface forcing decreased from -9.1 Wm^{-2} under clear sky to -6.2 Wm^{-2} under cloudy sky conditions. However, the difference in the aerosol atmospheric forcing for cloudy and clear sky was small, decreasing from 4.1 Wm^{-2} without clouds to 3.6 Wm^{-2} with clouds.

The clear and cloudy sky solar absorption was 292 and 244 Wm^{-2}, respectively. The difference was due to reflection of shortwave fluxes by clouds at the TOA, that is, shortwave cloud radiative forcing. The TOA cloud radiative forcing (Cf) is defined as the difference between net shortwave fluxes at the TOA

for cloudy and clear sky, which gives negative value since the clouds reflect the solar radiation back to space [e.g., *Kiehl and Ramanathan*, 1990; *Ramanathan et al.*, 1995]. The global mean TOA cloud forcing was -47.7 Wm^{-2}. The clear sky atmospheric absorption was 71 Wm^{-2} and the surface absorption was 221 Wm^{-2}. For a cloudy sky, the atmospheric absorption was 79 Wm^{-2} and the surface absorption was 165 Wm^{-2}. The global mean AOD was 0.15 and SSA was 0.95. The global mean clear sky aerosol forcing at the TOA and the surface were -5.0 and -9.1 Wm^{-2}, respectively. The presence of clouds decreased the negative TOA forcing from -5.0 Wm^{-2} to -2.6 Wm^{-2} and surface forcing from -9.1 Wm^{-2} to -6.2 Wm^{-2}. The aerosol atmospheric forcing was 4.1 Wm^{-2} without clouds and 3.6 Wm^{-2} with clouds. The planetary albedo was 0.29, while without clouds it was only 0.15.

6. ACKNOWLEDGMENTS

7. REFERENCES

Boucher, O., and D. Tanre, Estimation of the aerosol perturbation to the Earth's radiative budget over oceans using POLDER satellite aerosol retrievals, *Geophys. Res. Lett.*, *27*, 1103-1106, 2000.

Briegleb, P. Minnis, V. Ramanathan, and E. Harrison, Comparison of regional clear-sky albedos inferred from satellite observations and model computations, *J. Climate Appl. Meteor., 25*, 214-226, 1986.

Chen, T., W. B. Rossow, and Y. Zhang, Radiative effects of cloud-type variations, *J. Climate, 13*, 264-286, 2000.

Chou, M. D., P. K. Chan, and M. Wang, Aerosol radiative forcing derived from SeaWiFS-retrieved aerosol optical properties, *J. Atmos. Sci.*, *59*, 748-757, 2002.

Christopher, S. A., and J. Zhang, Shortwave aerosol radiative forcing from MODIS and CERES observations over the oceans, *Geophys. Res. Lett.*, *29*, doi:10.1029/2002GL014803, 2002.

Chung, C., V. Ramanathan, D. Kim, and I. Podgorny, Global Anthropogenic Aerosol Direct Forcing Derived from Satellite and Ground Based Observations, submitted to *J. Geophys. Res.,* 2005.

Clough, S. A., F. X. Kneizys, and R. W. Davies, Line shape and the water vapor continuum, *Atmos. Res.*, *23*, 229-241, 1989.

Diner, D. J., and Co-authors, Multiangle Imaging Spectroradiometer (MISR) description and experiment overview, *IEEE Trans. Geosci. Remote Sens.*, *36*, 1072-1087, 1998.

Dubovik, O., and M. D. King, A flexible inversion algorithm for retrieval of aerosol optical properties from Sun and sky radiance measurements, *J. Geophys. Res.*, *105*, 20,673-20,696, 2000.

Dubovik, O., A. Smirnov, B. N. Holben, M. D. King, Y. J. Kaufman, and I. Slutsker, Accuracy assessments of aerosol optical properties retrieved from AERONET Sun and sky radiance measurements, *J. Geophys. Res.*, *105*, 9791-9806, 2000.

Dubovik, O., B. N. Holben, T. F. Eck, A. Smirnov, Y. J. Kaufman, M. D. King, D. Tanre, and I. Slutsker, Variability of absorption and optical properties of key aerosol types observed in worldwide locations, *J. Atmos. Sci.*, *59*, 590-608, 2002.

Fu, Q., and K. N. Liou, On the correlated *k*-distribution method for radiative transfer in nonhomogeneous atmospheres, *J. Atmos. Sci.*, *49*, 2139-2156, 1992.

Harrison, E. F., P. Minnis, B. R. Barkstrom, V. Ramanathan, R. D. Cess, and G. G. Gibson, Seasonal Variation of Cloud Radiative Forcing Derived from the Earth Radiation Budget Experiment, *J. Geophys. Res.*, *95*, 18,687-18,703, 1990.

Haywood, J. M., and V. Ramaswamy, Global sensitivity studies of the direct radiative forcing due to anthropogenic sulfate and black carbon aerosols, *J. Geophys. Res.*, *103*, 6043-6058, 1998.

Hess, M., P. Koepke, and I. Schult, Optical Properties of Aerosols and clouds: The software package OPAC, *Bull. Am. Met. Soc.*, *79*, 831-844, 1998.

Holben, B. N., T. F. Eck, I. Slutsker, D. Tanré, J. P. Buis, A. Setzer, E. Vermote, J. A. Reagan, Y. J. Kaufman, T. Nakajima, F. Lavenu, I. Jankowiak and A. Smirnov, AERONET-A federated instrument network and data archive for aerosol characterization, *Rem. Sens. Environ.*, *66*, 1-16, 1998.

Holben, B. N., and Co-authors, An emerging ground-based aerosol climatology: Aerosol optical depth from AERONET, *J. Geophys. Res., 106*, 12,067-12,097, 2001.

Kahn, R., P. Banerjee, and D. McDonald, The sensitivity of multiangle imaging to natural mixtures of aerosols over ocean, *J. Geophys. Res.*, *106*, 18,219-18,238, 2001.

Kato, S., T. P. Ackerman, J. H. Mather, and E. E. Clothiaux, The *k*-distribution method and correlated-k approximation for a shortwave radiative transfer model, *J. Quant. Spectrosc. Radiat. Transfer*, *62*, 109-121, 1999.

Kiehl, J. T. and V. Ramanathan, Comparison of Cloud Forcing Derived from the Earth Radiation Budget Experiment with the NCAR Community Climate Model, *J. Geophys. Res.*, *95*, 11,679-11,698, 1990

Lacis, A. A., and V. Oinas, A description of the correlated *k* distribution method for modeling nongray gaseous absorption, thermal emission, and multiple scattering in vertically

inhomogeneous atmospheres, *J. Geophys. Res.*, *96*, 9027-9063, 1991.

Liao, H., and J. H. Seinfeld, Effects of clouds on direct aerosol radiative forcing of climate, *J. Geophys. Res.*, *103*, 3781-3788, 1998.

Liepert, B. G., Observed reductions of surface solar radiation at sites in the United States and worldwide from 1961 to 1990, *Geophys. Res. Lett.*, *29*, doi:10.1029/2002GL014910, 2002.

Martonchik, J. V., D. J. Diner, R. Kahn, B. Gaitley, and B. N. Holben, Comparison of MISR and AERONET aerosol optical depths over desert sites, *Geophys. Res. Lett.*, *31*, doi:10.1029/2004GL019807, 2004.

Myhre, G., A. Grini, J. M. Haywood, F. Stordal, B. Chatenet, D. Tanre, J. Sundet, and I. Isaksen, Modeling the radiative impact of mineral dust during the Saharan Dust Experiment (SHADE) campaign, *J. Geophys. Res.*, *108*, doi:10.1029/2002JD002566, 2003.

Ohmura, A., and M. Wild, Is the Hydrological Cycle Accelerating?, *Science*, 298, 1345-1346, 2002.

Podgorny, I. A., W. C. Conant, V. Ramanathan, and S. K. Satheesh, Aerosol modulation of atmospheric and solar heating over the tropical Indian Ocean, *Tellus*, *52B*, 947-958, 2000.

Podgorny, I. A., and V. Ramanathan, A modeling study of the direct effect of aerosols over the Tropical Indian Ocean, *J. Geophys. Res.*, *106***, 24,097-24,105, 2001.

Ramanathan, V., R. D. Cess, E. F. Harrison, P. Minnis, B. R. Barkstrom, E. Ahmad, and D. Hartmann, Cloud-Radiative Forcing and Climate: Results from the Earth Radiation Budget Experiment, *Science*, *243*, 57-63, 1989.

Ramanathan, V., B. Subasilar, G. J. Zhang, W. Conant, R. D. Cess, J. T. Kiehl, H. Grassl, and L. Shi, Warm pool heat budget and shortwave cloud forcing: A missing physics?, *Science*, *267*, 499-503, 1995.

Ramanathan, V., and Co-authors, The Indian Ocean Experiment: An integrated analysis of the climate forcing and effects of the Great Indo-Asian Haze, *J. Geophys. Res., 106*, 28,371-28,398, 2001.

Ramanathan, V., C. Chung, D. Kim, T. Bettge, L. Buja, J. T. Kiehl, W. M. Washington, Q. Fu, D. R. Sikka, and M. Wild, Atmospheric brown clouds: Impacts on South Asian climate and hydrological cycle, *PNAS*, *102*, 15, 5326-5333, 2005.

Roderick, M. L., and G. D. Farquhar, The Cause of Decreased Pan Evaporation over the Past 50 Years, *Science*, *298*, 1410-1411, 2002

Rossow, W. B., and R. A. Schiffer, Advances in understanding clouds from ISCCP, *Bull. Amer. Meteor. Soc.*, *80*, 2261-2287, 1999.

Rotstayn, L., and U. Lohmann, Tropical rainfall trends and the indirect aerosol effect, *J. Climate*, *15*, 2103-2116, 2002.

Satheesh, S. K., V. Ramanathan, Xu Li-Jones, J. M. Lobert, I. A. Podgorny, J. M. Prospero, B. N. Holben, and N. G. Loeb, A model for the natural and antropogenic aerosols over the tropical

Indian Ocean derived from Indian Ocean Experiment data, *J. Geophys. Res., 104,* 27,421-27,440, 1999.

Stanhill, G., S. Cohen, Global dimming: a review of the evidence for a widespread and significant reduction in global radiation with discussion of its probable causes and possible agricultural consequences, *Agric. Forest Meteorol., 107*, 255–278, 2001.

Stephens, G. L., and S. C. Tsay, On the cloud absorption anomaly, *Q. J. R. Meterol. Soc.*, *116*, 671-704, 1990

Vogelmann, A. M., V. Ramanathan, W. C. Conant, and W. E. Hunter, Observational constraints on non-Lorentzian continuum effects in the near-infrared solar spectrum using ARM ARESE Data, *J. Quant. Spectrosc. Radiat. Transfer, 60*, 231-246, 1998.

Vogelmann, A. M., V. Ramanathan, and I. A. Podgorny, Scale dependence of solar heating rates in convective cloud systems with implications to General Circulation Models, *J. Climate*, *14*, 1738-1752, 2001.

Yu, H., R. E. Dickinson, M. Chin, Y. J. Kaufman, M. Zhou, L. Zhou, Y. Tian, O. Dubovik and B. N. Holben, Direct radiative effect of aerosols as determined from a combination of MODIS retrievals and GOCART simulations, *J. Geophys. Res.*, *109*, doi:10.1029/2003JD03206, 2004.
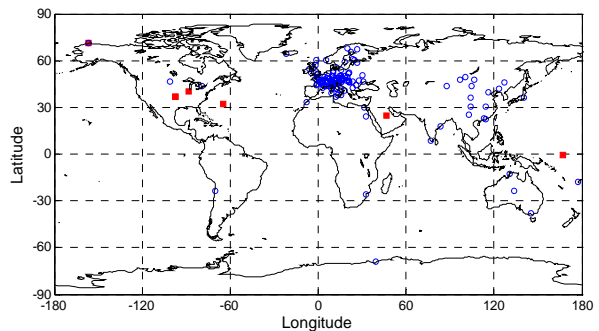
Fig. 1: The location of BSRN and GEBA stations for validation of MACR radiative transfer model during the period from 2000 to 2002. Red square represents the BSRN stations, and blue circle represents the GEBA stations.
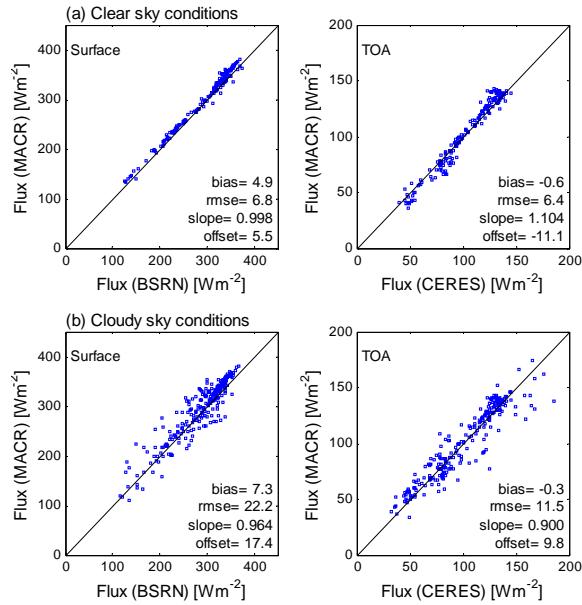
Fig. 2: Comparison of diurnal mean global fluxes between MACR model and BSRN measurements under (a) clear and (b) cloudy sky conditions.
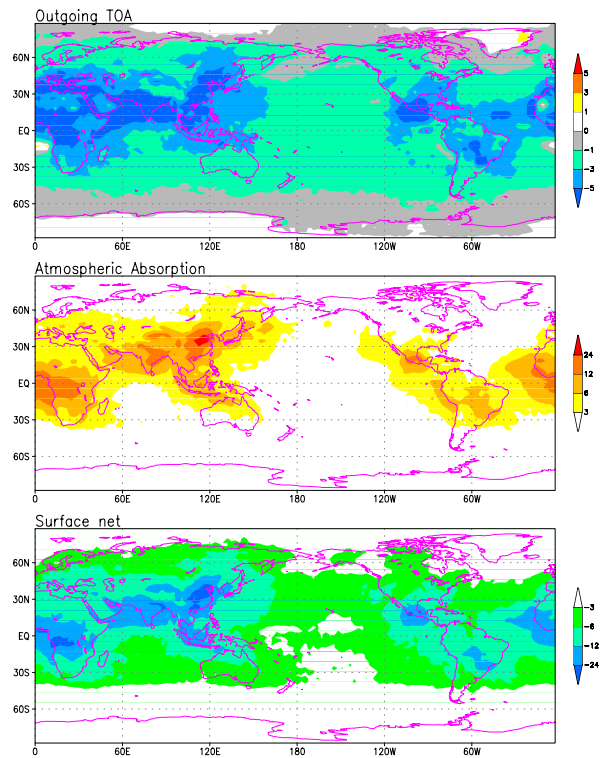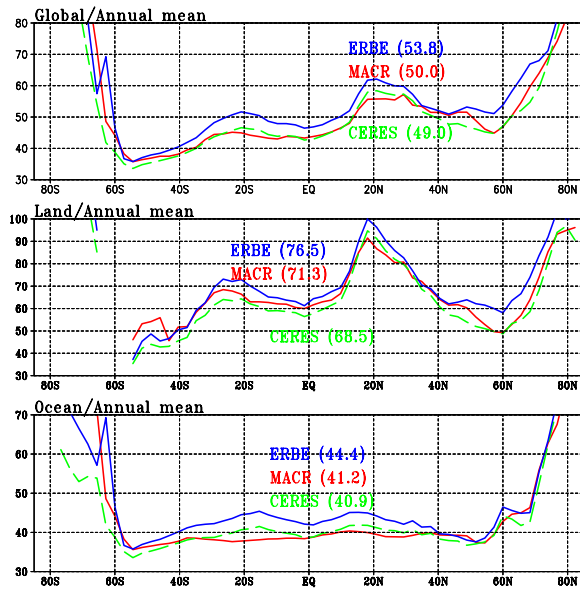

Fig. 3: Comparison of the MACR estimated zonal mean TOA fluxes with satellite retrievals (CERES and ERBE) over the globe (top panel), land (middle panel), and ocean (bottom panel) under clear sky conditions. Blue line represents the observations from the ERBE (1985-1989 average), green line represents the observations from the CERES (2000-2002 average), and red line represents the MACR estimates given in Wm^{-2}.

Fig. 4: Annual mean cloudy sky aerosol radiative forcing at the TOA (top panel), vertically integrated forcing in the atmosphere (middle panel), forcing at the surface (bottom panel). The forcing is calculated without cloud effects (clear sky forcing) given in Wm^{-2}.